Article

Cell Reports

Dynein Transmits Polarized Actomyosin Cortical Flows to Promote Centrosome Separation

Graphical Abstract

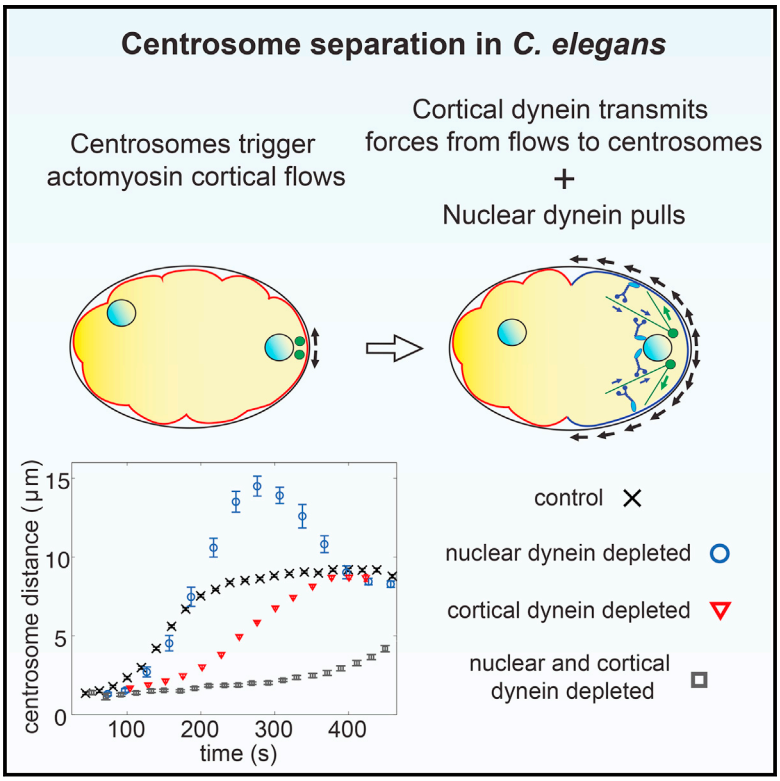

Highlights

- Nuclear dynein and cortical dynein together separate centrosomes
- Polarized actomyosin cortical flows promote centrosome separation
- Cortical dynein transmits forces from cortical actomyosin flows to centrosomes

Authors

Alessandro De Simone, François Nédélec, Pierre Gönczy

Correspondence

pierre.gonczy@epfl.ch

In Brief

Accurate centrosome separation is fundamental for robust spindle assembly. Using cell biological and computational approaches, De Simone et al. show that centrosome separation in *C. elegans* embryos is driven by nuclear dynein, together with cortical dynein, the latter acting as a coupling device that transmits forces produced by polarized cortical actomyosin flows.

De Simone et al., 2016, Cell Reports *14*, 2250–2262
March 8, 2016
http://dx.doi.org/10.1016/j.celrep.2016.01.077

OPEN ACCESS
CellPress

Cell Reports
Article

Dynein Transmits Polarized Actomyosin Cortical Flows to Promote Centrosome Separation

Alessandro De Simone,[1] François Nédélec,[2] and Pierre Gönczy[1,*]
[1]Swiss Institute for Experimental Cancer Research (ISREC), School of Life Sciences, Swiss Federal Institute of Technology (EPFL), 1015 Lausanne, Switzerland
[2]Cell Biology and Biophysics Unit, European Molecular Biology Laboratory (EMBL), Meyerhofstrasse 1, 69117 Heidelberg, Germany
*Correspondence: pierre.gonczy@epfl.ch
http://dx.doi.org/10.1016/j.celrep.2016.01.077

SUMMARY

The two centrosomes present at the onset of mitosis must separate in a timely and accurate fashion to ensure proper bipolar spindle assembly. The minus-end-directed motor dynein plays a pivotal role in centrosome separation, but the underlying mechanisms remain elusive, particularly regarding how dynein coordinates this process in space and time. We addressed these questions in the one-cell *C. elegans* embryo, using a combination of 3D time-lapse microscopy and computational modeling. Our analysis reveals that centrosome separation is powered by the joint action of dynein at the nuclear envelope and at the cell cortex. Strikingly, we demonstrate that dynein at the cell cortex acts as a force-transmitting device that harnesses polarized actomyosin cortical flows initiated by the centrosomes earlier in the cell cycle. This mechanism elegantly couples cell polarization with centrosome separation, thus ensuring faithful cell division.

INTRODUCTION

Centrosomes are the major microtubule-organizing centers of most animal cells and are critical for directing assembly of the mitotic spindle and, thus, for faithful chromosome segregation. A prerequisite for proper bipolar spindle assembly is the timely separation of the two centrosomes present at the onset of mitosis (reviewed in Tanenbaum and Medema, 2010). Centrosome separation typically occurs along the nuclear envelope, but the underlying mechanisms remain incompletely understood in many cases.

Microtubule-associated motor proteins of the kinesin-5 family are required for centrosome separation in several systems (reviewed in Ferenz et al., 2010). These tetrameric plus-end-directed motors can push centrosomes apart by cross-linking and sliding overlapping antiparallel microtubules located between them. However, kinesin-5 is partially dispensable for centrosome separation in some systems and completely dispensable in others, including *C. elegans* (Raaijmakers et al., 2012; Saunders et al., 2007; Tikhonenko et al., 2008). Therefore, distinct mechanisms that do not rely on kinesin-5 motors must exist. The minus-end-directed microtubule-associated motor dynein is an important contributor in this respect. Thus, dynein separates centrosomes in human cells with compromised kinesin-5 function (Raaijmakers et al., 2012). Furthermore, dynein is absolutely essential for centrosome separation in several species, including *C. elegans* and *Drosophila* (Gönczy et al., 1999; Robinson et al., 1999), raising the possibility that this represents an ancestral separation mechanism (reviewed in Dujardin and Vallee, 2002). The mechanisms by which dynein governs centrosome separation are only partially understood.

Dynein is present throughout the cytoplasm, where it can exert length-dependent forces on centrosomes while carrying cargos along microtubules or being bound to a stable cytoplasmic substrate (reviewed in Reinsch and Gönczy, 1998; Tanenbaum and Medema, 2010). For instance, in the one-cell *C. elegans* embryo, the cytoplasmic pool of dynein is responsible for the centration of the two pronuclei that occurs shortly after centrosome separation (Kimura and Onami, 2005). In addition, dynein is enriched in different sub-cellular locations, including on the cytoplasmic face of the nuclear envelope and at the cell cortex below the plasma membrane (Gönczy et al., 1999; Splinter et al., 2010; reviewed in Kotak and Gönczy, 2013). Overall, owing to these multiple localizations, it is not clear where dynein acts to power centrosome separation.

One model posits that dynein uniformly distributed on the nuclear envelope could separate centrosomes by pulling on microtubules emanating from them (Gönczy et al., 1999). In line with this view, dynein anchored on the nuclear envelope contributes to centrosome separation in human cells when kinesin-5 function is partially compromised (Raaijmakers et al., 2012). However, whether this reflects the mechanism by which dynein contributes to centrosome separation in unperturbed conditions is not known. Moreover, nuclear dynein is not essential for centrosome separation in *C. elegans*, as evidenced by the fact that centrosomes move apart in embryos depleted of the nuclear-envelope hook protein ZYG-12, in which dynein does not localize to the nucleus (Malone et al., 2003). Similarly, hypomorphic mutations of the dynein heavy chain can lead to centrosome detachment in *Drosophila* embryos yet result only in partial impairment of centrosome separation (Robinson et al., 1999). Overall, the exact contribution of nuclear dynein to centrosome separation remains to be clarified.

An alternative model posits that dynein anchored at the cell cortex could drive centrosome separation by using its

minus-end-directed motor activity to pull on astral microtubules abutting the cortex (reviewed in Dujardin and Vallee, 2002). Compatible with this possibility, cortical dynein pulls on astral microtubules to position the mitotic spindle in several systems (reviewed in Kotak and Gönczy, 2013). In *Drosophila* embryos, a mathematical model indicates that, in principle, cortical dynein pulling on astral microtubules can drive centrosome separation, provided there is a mechanism to ensure that the net force exerted on one centrosome is directed away from the other (Cytrynbaum et al., 2005). The exact nature of such a mechanism is not known, although the observed spatial asymmetry of microtubule aster organization or a postulated asymmetry in dynein activity could be responsible (Cytrynbaum et al., 2005).

The actomyosin network also plays a role in centrosome separation in some systems. Thus, actin dynamics are required for centrosome separation in *Drosophila* embryos, although contractility of the actomyosin network is not needed, so that the mechanisms underlying this requirement are not clear (Cao et al., 2010). By contrast, actomyosin contractility is required in the minority of vertebrate Ptk2 cells in which centrosomes move apart only after nuclear envelope breakdown (Rosenblatt et al., 2004). How actomyosin contractility-based forces are transmitted to microtubules to move centrosomes in this case is not known. Furthermore, it is unclear how the pattern of actomyosin-network cortical flow could ensure that the two centrosomes always move in opposite directions.

Overall, the mechanisms by which dynein and the actomyosin network contribute to centrosome separation, as well as those by which this process is coordinated in time and space, remain incompletely understood. The one-cell-stage *C. elegans* embryo is particularly well suited to address these questions, because it relies strictly on dynein to separate centrosomes (Gönczy et al., 1999), thus allowing analysis without the potentially confounding effects of kinesin-5 (Saunders et al., 2007). We set out to dissect centrosome separation in this system, using a combination of 3D time-lapse microscopy and computational modeling.

RESULTS

Centrosome Separation in One-Cell-Stage *C. elegans* Embryos

The *C. elegans* one-cell-stage embryo becomes polarized along the anterior-posterior (A-P) axis shortly after fertilization (Figure 1A; Movie S1). Initially, the male pronucleus is located on the presumptive posterior side, and the female pronucleus is located on the future anterior side (Figure 1A, 57 s). As in other systems, the sperm contributes the sole pair of centrioles to the zygote in *C. elegans*, so that the two centrosomes present at the onset of mitosis are associated with the male pronucleus, positioned near the cell cortex (Figure 1A, 57 s). Centrosome separation begins during early prophase and occurs along the surface of the male pronucleus (Figure 1A, 225 s). Thereafter, the two pronuclei migrate toward each other and meet in the embryo center (Figure 1A, 333 s and 369 s).

To decipher the mechanisms governing centrosome separation, we performed high temporal and spatial resolution 3D time-lapse microscopy of one-cell-stage embryos expressing the centrosomal marker GFP::TAC-1 (otherwise wild-type, hereinafter referred to as "control") (Bellanger and Gönczy, 2003; Le Bot et al., 2003; Srayko et al., 2003). We tracked centrosomes using GFP fluorescence and developed an algorithm to automatically detect the position and size of pronuclei using differential interference contrast (DIC) microscopy (Figure 1A). Analysis of centrosome-centrosome distances revealed that centrosome separation can be described as occurring in three phases (Figures 1B and 1C): an initial phase during which centrosomes start moving apart (onset); an intermediate phase with maximal velocity, during which most of the separation occurs (separation); and a final equilibrium phase, during which separation slows down significantly and almost stops (equilibrium). A slight augmentation of centrosome-centrosome distance occurs also during that equilibrium time, potentially because the male pronucleus grows as the cell-cycle progresses, thus pushing centrosomes apart (Figures 1D and 1E).

Nuclear and Cortical Dynein Cooperate to Ensure Timely Centrosome Separation

We set out to decipher the nature of the forces that move centrosomes apart during the separation phase. Dynein is enriched slightly on the nuclear envelope and on the cell cortex in the one-cell embryo and is essential for centrosome separation (Gönczy et al., 1999) (Figures S1A and S1B). We began by investigating, in a quantitative manner, whether dynein located on the nuclear envelope contributes to centrosome separation by depleting ZYG-12, which is necessary to anchor dynein on the surface of the nucleus (Malone et al., 2003). We found that the centrosomes detach from the male pronucleus in *zyg-12(ct350)* mutant embryos and separate from one another, as previously reported (Malone et al., 2003). Strikingly, in addition, our analysis uncovered that centrosomes do not separate normally in these embryos but instead undergo excess separation along the cortex (Figures 2C, 2D, and 2I; Table S1; Movie S2). Thereafter, centrosomes approach each other while moving toward the cell center, likely reflecting the action of centering forces that are known to act at this later stage (Kimura and Onami, 2005). Overall, these results reveal that, in the absence of nuclear dynein, the path of centrosome separation differs strikingly from that in control embryos. We conclude that nuclear dynein plays a critical role in limiting the extent of, and in imposing spatial constraints on, centrosome separation.

We set out to decipher the mechanisms governing excess centrosome separation in *zyg-12(ct350)* mutant embryos. To verify that dynein is needed, we depleted the dynein heavy-chain DHC-1 by RNAi in *zyg-12(ct350)* mutant embryos. As anticipated, we found that centrosome separation is completely abolished in such embryos, demonstrating that centrosome movements in *zyg-12(ct350)* mutant embryos are dynein dependent (Figures S1C and S1D). Which pool of dynein drives excess centrosome separation in such embryos? We reasoned that cortical dynein is a likely candidate, because excess separation occurs along the cell cortex in *zyg-12(ct350)* mutant embryos (Figure 2D; Movie S2). Cortical anchoring of dynein during mitosis in one-cell *C. elegans* embryos depends upon the heterotrimeric Gα proteins GOA-1 and GPA-16, as well as on their interacting partners GPR-1/2 and LIN-5 (Colombo et al., 2003;

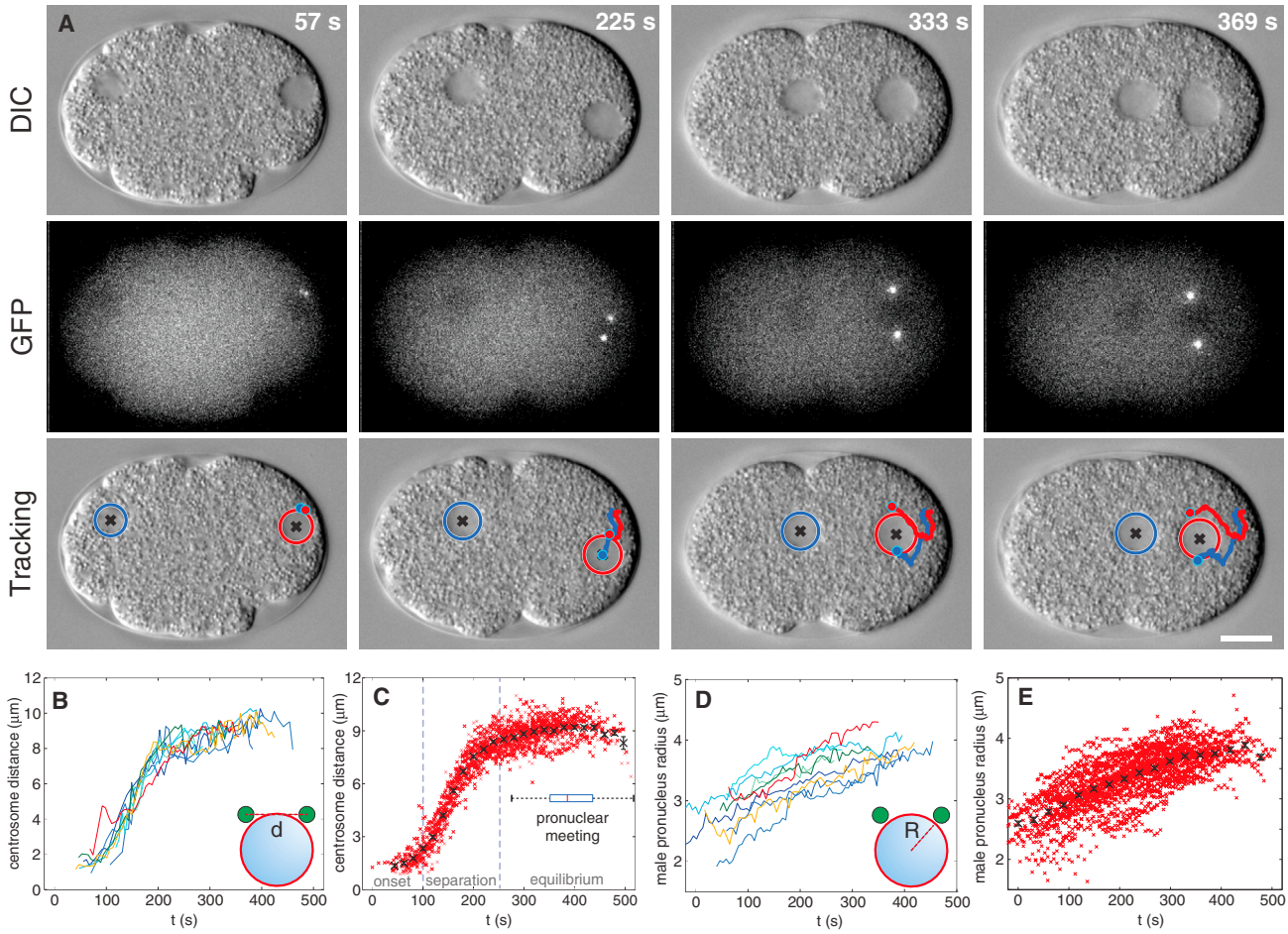

Figure 1. Centrosome Separation in One-Cell *C. elegans* Embryo

(A) Centrosome separation monitored with 3D time-lapse DIC (top panels) and GFP fluorescent microscopy (middle panels show z-maximum projections) in embryos expressing GFP::TAC-1, together with tracking of centrosomes over the entire separation process (bottom panels). Here and in the following figures, in the tracking images, centrosomes (blue and red dots: z-projection of the 3D positions of centrosomes onto the displayed DIC image) are represented with their trajectories (blue and red tracks: z-projections). Pronuclei are highlighted (blue disk: female pronucleus; red disk: male pronucleus; black crosses: z-projection of the 3D positions of pronuclei centers onto the displayed DIC image). Here and in the following figures, time is indicated in seconds, and control embryos have been synchronized by maximizing the overlap of centrosome-centrosome distance curves, with 0 s defined as the earliest time point at which two distinct centrosomes could be detected in the whole synchronized control dataset (Experimental Procedures). Scale bar, 10 μm.

(B) Centrosome-centrosome distance (d) as a function of time for nine representative embryos.

(C) Average centrosome-centrosome distance as a function of time (n = 42 embryos). Separation distances for individual embryos (red crosses) and average with SEM (black crosses) are depicted. The box plot represents the timing of pronuclear meeting (quartiles are represented).

(D) Male pronucleus radius (R) as a function of time for nine representative embryos.

(E) Average male pronucleus size as a function of time. Male pronucleus radius for individual embryos (red crosses) and average with SEM (black crosses) are depicted. See also Movie S1.

Gotta and Ahringer, 2001; Gotta et al., 2003; Lorson et al., 2000; Nguyen-Ngoc et al., 2007; Srinivasan et al., 2003; Tsou et al., 2002). Therefore, to test the requirement for cortical dynein in the excess centrosome separation that occurs upon impaired *zyg-12* function, we analyzed *goa-1/gpa-16(RNAi) zyg-12(ct350)* embryos. Strikingly, we found that excess centrosome movements are prevented and that centrosome separation is strongly impaired in such embryos (Figures 2E, 2F, and 2I; Table S1; Movie S3). We also noted that centrosomes move apart from one another at a later time, when they center toward the embryo middle (Figure 2F), again likely reflecting centering forces acting at this later stage. Moreover, we found that the sole depletion of cortical dynein by *goa-1/gpa-16(RNAi)* slows down centrosome separation (Figures 2G–2I; Table S1; Movie S4). Analogous results were obtained with *lin-5(RNAi) zyg-12(ct350)* and *lin-5(RNAi)* embryos (Figure S2A; Table S1). Together, these findings indicate that cortical dynein plays a partially redundant role in centrosome separation, with nuclear dynein likely being responsible for the remaining movement. Overall, these results led us to conclude that proper centrosome separation in one-cell *C. elegans* embryos results from the combined contributions of dynein acting at the nuclear envelope and at the cell cortex.

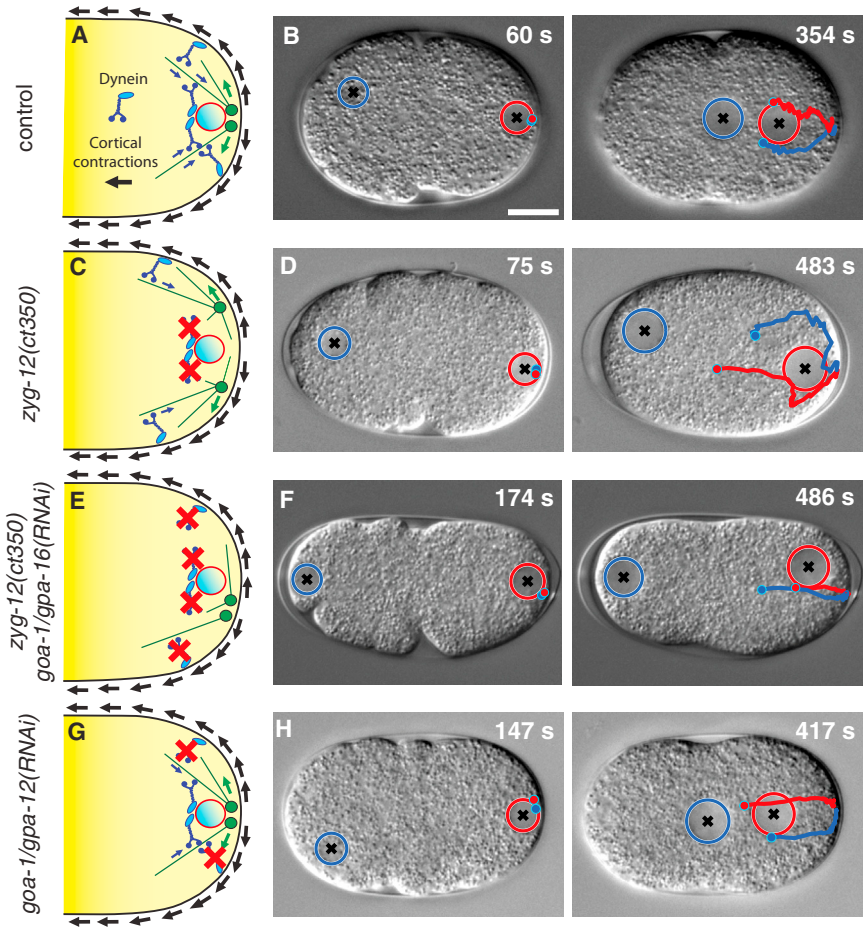

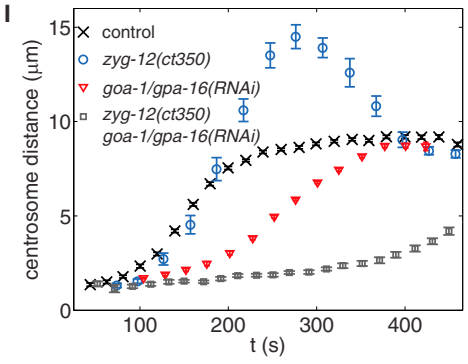

Figure 2. Cortical and Nuclear Dynein Separate Centrosomes

(A–H) Schematics (A, C, E, and G) and snapshots (B, D, F, and H) of centrosome separation in control and indicated RNAi/mutant conditions (left: onset of separation, right: moment preceding pronuclear meeting or equivalent time; Experimental Procedures). Here and in the following figures, in the schematics, the posterior part of the embryo is represented together with the male pronucleus (blue disk with red contour), centrosomes (green dots), microtubules (green lines), dynein motors (blue complexes), dynein anchors (blue ellipses), and cortical flows (black arrows). Depleted motors are indicated with red crosses. Scale bar, 10 µm.

(I) Average centrosome-centrosome distance with SEM as a function of time in the indicated RNAi/mutant conditions. Number of embryos analyzed: control, n = 42 (same as Figure 1); *goa-1/gpa-16(RNAi)*, n = 20; *zyg-12(ct350)*, n = 10; *zyg-12(ct350) goa-1/gpa-16(RNAi)*, n = 16. Here and in the following figures, embryos from the same experimental condition have been synchronized by maximizing the overlap of centrosome-centrosome separation curves. Average curves from each experimental condition have been synchronized with that of the control, using the average male pronucleus radius as a time reference (Experimental Procedures), with time 0 s defined as the earliest time point at which two separate centrosomes could be detected in the whole synchronized control dataset.

See also Figures S1 and S2 and Movies S2, S3, and S4.

Actomyosin Contractions Power Cortical Dynein-Mediated Centrosome Separation

How does cortical dynein contribute to centrosome separation? One possibility is that motor activity is needed to pull on astral microtubules at the cortex. Alternatively, given that the contractile cortical actomyosin network flows toward the anterior at the very same time that centrosomes separate (reviewed in Rose and Gönczy, 2014), we reasoned that cortical dynein could serve as a coupling device to transmit forces from the actomyosin cortex to centrosomes. Interestingly, the centrosomes themselves trigger the actomyosin flow, so that the pattern of flow is always directed away from them (Bienkowska and Cowan, 2012; Goldstein and Hird, 1996; Munro et al., 2004).

We set out to test this coupling model by impairing actomyosin contractility through depletion of the non-muscle myosin NMY-2 in *zyg-12(ct350)* mutant embryos. Depleting NMY-2 by RNAi does not impair cortical dynein distribution either in the wild-type or in embryos expressing YFP::GPR-1, which were utilized to increase baseline levels of cortical DHC-1 (Figure S3). Importantly, we found that, as for *goa-1/gpa-16(RNAi) zyg-12(ct350)* embryos, excess centrosome movements are prevented, and overall centrosome separation is strongly impaired in *nmy-2(RNAi) zyg-12(ct350)* embryos (Figures 3A, 3B, and 3E; Table S1; Movie S5). The slightly less penetrant phenotype compared to *goa-1/gpa-16(RNAi) zyg-12(ct350)* (compare Figure 2I with Figure 3E, past 300 s) could be due to incomplete NMY-2 depletion by RNAi or could reflect an NMY-2-independent contribution of cortical dynein to centrosome separation. Regardless, as for *goa-1/gpa-16(RNAi)*, we found that the sole depletion of NMY-2 significantly slows down centrosome separation (Figures 3C–3E;

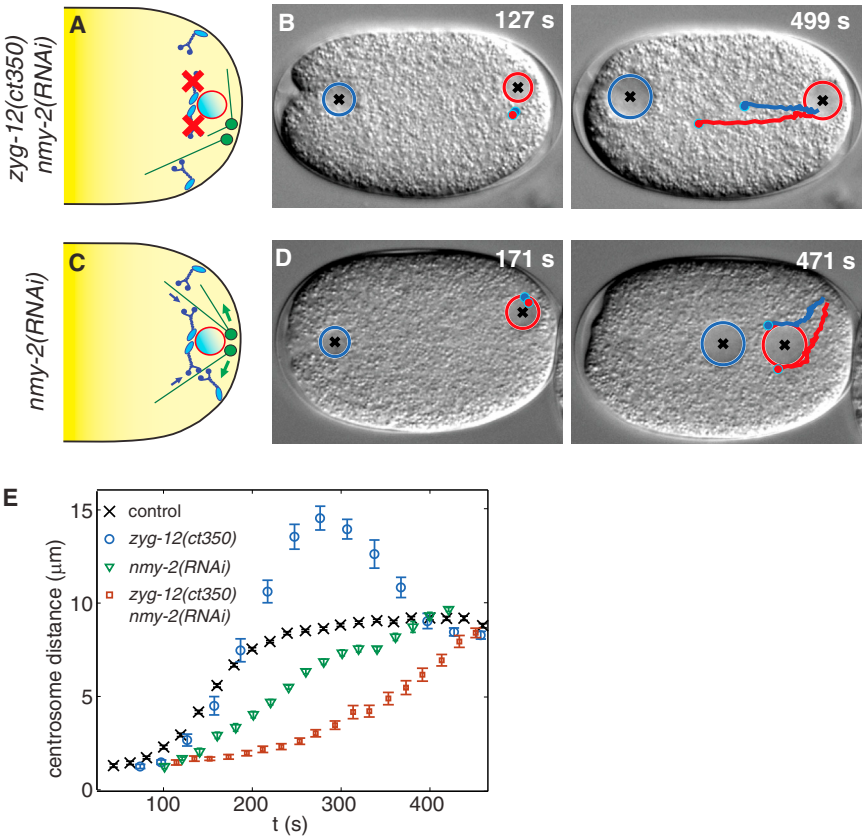

Figure 3. Actomyosin Contractility Promotes Centrosome Separation

(A–D) Schematics (A and C) and snapshots (B and D) of centrosome separation in control and indicated RNAi conditions (left: onset of separation; right: moment preceding pronuclear meeting or equivalent time). Scale bar, 10 μm.

(E) Average centrosome-centrosome distance with SEM as a function of time in the indicated RNAi/mutant conditions. Number of embryos analyzed: control, n = 42 (same as Figure 1); *zyg-12(ct350)*, n = 10 (same as Figure 2); *nmy-2(RNAi)*, n = 10; *zyg-12(ct350) nmy-2(RNAi)*, n = 19.

See also Figures S2 and S3 and Movies S5 and S6.

Table S1; Movie S6). We verified also that the rate of pronuclear growth is not altered in *nmy-2(RNAi)* embryos, suggesting that slowing down of centrosome separation is not due merely to delayed cell-cycle progression (Figure S2B). Furthermore, similar results were obtained by depleting RHO-1, which also promotes contractility of the actomyosin network (Motegi and Sugimoto, 2006) (Figure S2C; Table S1). Overall, these results lead us to conclude that contractility of the actomyosin network is critical for proper centrosome separation.

Dynein Couples Actomyosin Cortical Flow with Centrosome Separation

If anteriorly directed cortical actomyosin flows provide separation forces and dynein serves to transmit these forces, then the flow of cortical dynein should be similar to that of the cortical actomyosin network itself. To test this prediction of the coupling model, we used particle image velocimetry to measure in the same embryos the flow of cortical dynein complexes using YFP::GPR-1 and of the actomyosin network using Lifeact::mKate2 (Mayer et al., 2010) (Figure 4A; Movie S7). As shown in Figure 4B, these experiments revealed that, at each time point, the local flow of YFP::GPR-1 strongly correlates with that of Lifeact::mKate2 (Pearson coefficient $\rho = 0.76$; $p < 10^{-38}$). Likewise, the direction of the local flow vectors is extremely similar between the two fusion proteins (Figure 4C). These findings are fully compatible with the notion that cortical dynein complexes are transported by the flow of the actomyosin cortex.

We reasoned that, if cortical dynein indeed serves as a linker that transmits forces generated by anteriorly directed cortical actomyosin flows, then in the absence of nuclear dynein, the velocities of centrosome separation should correlate with those of cortical actomyosin flows. Note that, even though an overall correlation is expected, substantial deviation in centrosome separation velocities is anticipated owing to variability, for example, in centrosome position, microtubule aster organization, and cortical motor distribution. Nevertheless, we tested this prediction by measuring the velocities of centrosome separation and of cortical flows simultaneously using GFP::TAC-1 and GFP::NMY-2 in embryos depleted of nuclear dynein via *zyg-12(RNAi)* (Figure 5A; Movie S8). We found that, at each time interval, centrosome separation velocities exhibit a mild, but significant, correlation with local cortical flow velocities (Figure 5B; $\rho = 0.17$; $p = 0.03$). Furthermore, we found a stronger correlation when average centrosome separation velocities and cortical flows are considered over the entire imaging period in each embryo (Figure 5E; $\rho = 0.47$; $p = 0.02$).

We set out to further uncover the root of this correlation. We reasoned that, since cortical flows are imaged at the surface of the ellipsoidal embryo that is closest to the lens, if the overall correlation results from the specific action of actomyosin cortical flows on centrosomes through cortical dynein and microtubules, then a stronger correlation with cortical flows should be observed for the centrosome that is the closest to the imaged cortical plane (see Figure 5A). To test this prediction, we measured separately the contribution of the two centrosomes to the separation process (see Experimental Procedures). Strikingly, this analysis revealed that, at each time interval, local cortical flows are highly correlated with the movements of the closest centrosome (Figure 5C; $\rho = 0.34$; $p = 3 \cdot 10^{-5}$), but not with those of the furthest one (Figure 5D; $\rho = -0.12$; $p = 0.19$ [not significant; ns]). Furthermore, this differential correlation is even more pronounced when considering the averaged cortical flows and average centrosome movements in each embryo (Figures 5F and 5G; closest, $\rho = 0.68$; $p = 5 \cdot 10^{-4}$; furthest, $\rho = 0.04$; $p = 0.88$ [ns]).

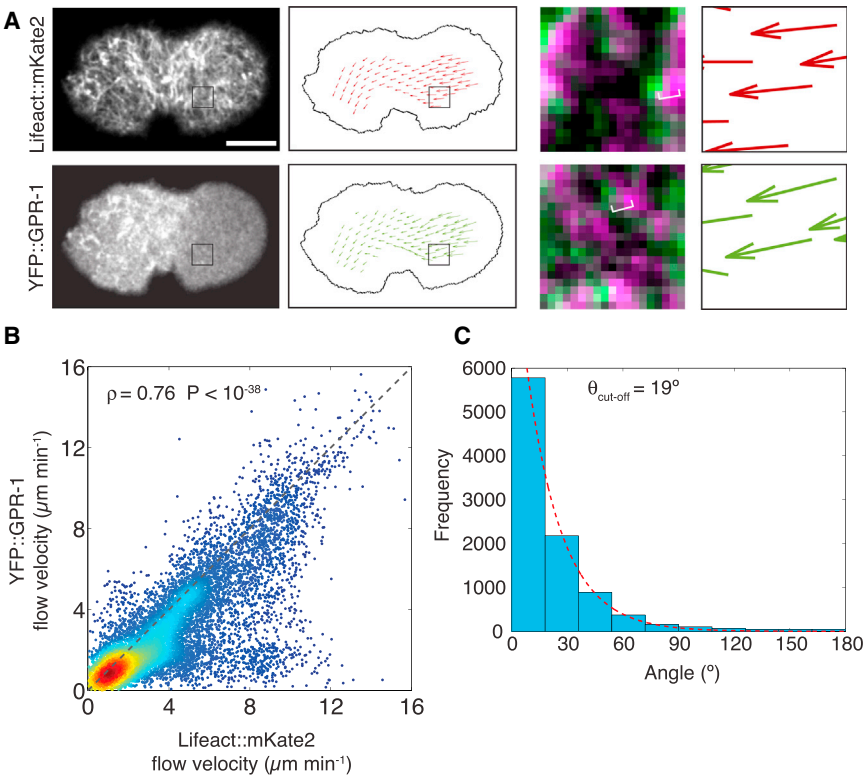

Figure 4. Correlated Flows of Cortical Actomyosin Network and Cortical Dynein Anchors

(A) Imaging and measurement of cortical flows of the actomyosin network (top, Lifeact::mKate2) and of cortical dynein anchors (bottom, YFP::GPR-1) during centrosome separation in the same embryo. A snapshot of cortical distribution is shown (left panel) together with the measured flow velocity field (right panel). Insets: two successive frames are superimposed (magenta and green, respectively), with brackets exemplifying focal protein enrichments that changed position between the two time frames. In the PIV images, arrow direction and length represent flow direction and velocity, respectively (a.u.). Scale bar, 10 μm. (B and C) Correlation of instantaneous local flows of Lifeact::mKate2 and YFP::GPR-1. (B) YFP::GPR-1 flow velocity is represented as a function of Lifeact::mKate2 flow velocity in the same position. Flow velocities are highly correlated (n = 10 embryos, ten time frames per embryo, Pearson correlation coefficient $\rho = 0.76$, $p < 10^{-38}$, Student's t test). Data points are represented with a scale of color dependent on their spatial density in the scatterplot (a.u., from sparser to denser: blue, light blue, green, yellow, red, and dark red). (C) Distribution of angles between Lifeact::mKate2 and YFP::GPR-1 flow directions in the same dataset. The angle distribution is peaked at $\theta = 0°$, and decays exponentially (cutoff angle, 19°). The probability that two independent velocity fields result in the observed angle distribution is $p < 10^{-38}$.

We excluded from the analysis those flow vectors with an initial PIV window that is partially outside the segmented region of the embryo, as represented in (A), to minimize discrepancies in the flow fields due to detection errors (Supplemental Experimental Procedures). However, analogous conclusions are reached when all the velocity vectors within the segmented embryo region are considered (correlation flow velocities, $\rho = 0.61$, $p < 10^{-38}$ (t test); cutoff angle, 25°). See also Movie S7.

Another expectation of the coupling model is that the correlation between the cortical actomyosin flows and the movements of the closest centrosome should be maximal close to the posterior pole of the embryo where centrosomes are located, and we found this to be the case indeed (Figure 5H). Overall, this analysis demonstrates that the correlation between cortical flows and centrosome separation results from a local interaction between the actomyosin cortical flows and the nearby centrosome. Taken together, these findings suggest that cortical dynein acts as a linker that transmits forces produced by anteriorly directed actomyosin-dependent flows to separate centrosomes.

Computational Model of Centrosome Separation

Is the action of dynein on the nuclear envelope combined with the cortical coupling device sufficient to explain centrosome separation? To address this question, we developed a computational model of centrosome separation in one-cell *C. elegans* embryos, using the cytoskeleton simulation engine Cytosim (Nedelec and Foethke, 2007) (Figure 6; Figure S4). We focused on the "separation" phase prior to reaching equilibrium (see Figure 1C), thus not including the centering forces, which are not the focus of this study.

In the computational model, overdamped Langevin equations are used to describe the movements of microtubules and pronuclei in a viscous fluid in the presence of Brownian motion. Centrosomes nucleate microtubules, which undergo dynamic instability with rates that depend on the applied force. Microtubules can interact with dynein motors located at the nuclear envelope and at the cell cortex. A given density of dynein motors is evenly distributed on the pronuclear surfaces, while cortical motors are present in excess and are also evenly distributed on the cell cortex; only active cortical motors are simulated. Both nuclear and cortical dynein motors move along bound microtubules and exert forces with a linear force-velocity relationship. Moreover, cortical motors flow toward the anterior, reflecting the effect of anteriorly directed actomyosin contractions, with a velocity tangential to the cell cortex that increases linearly from the anterior to the posterior. All simulation parameters are set using measured values when possible or varied within a reasonable range (Table S2).

Given that the densities of dynein motors at the nucleus and at the cortex are not known, we fitted these two parameters by using simultaneously the control, *goa-1/gpa-16(RNAi)*, and *zyg-12(ct350)* separation curves. Remarkably, such simultaneous fitting yielded very good qualitative and quantitative agreement between the simulations and the experimental data (Figure 6). Thus, in the simulations, centrosomes separate with a pace comparable with that observed experimentally in control embryos that have both cortical and nuclear motors (Figures 6A and 6B; Movie S9); moreover, centrosomes undergo excess separation

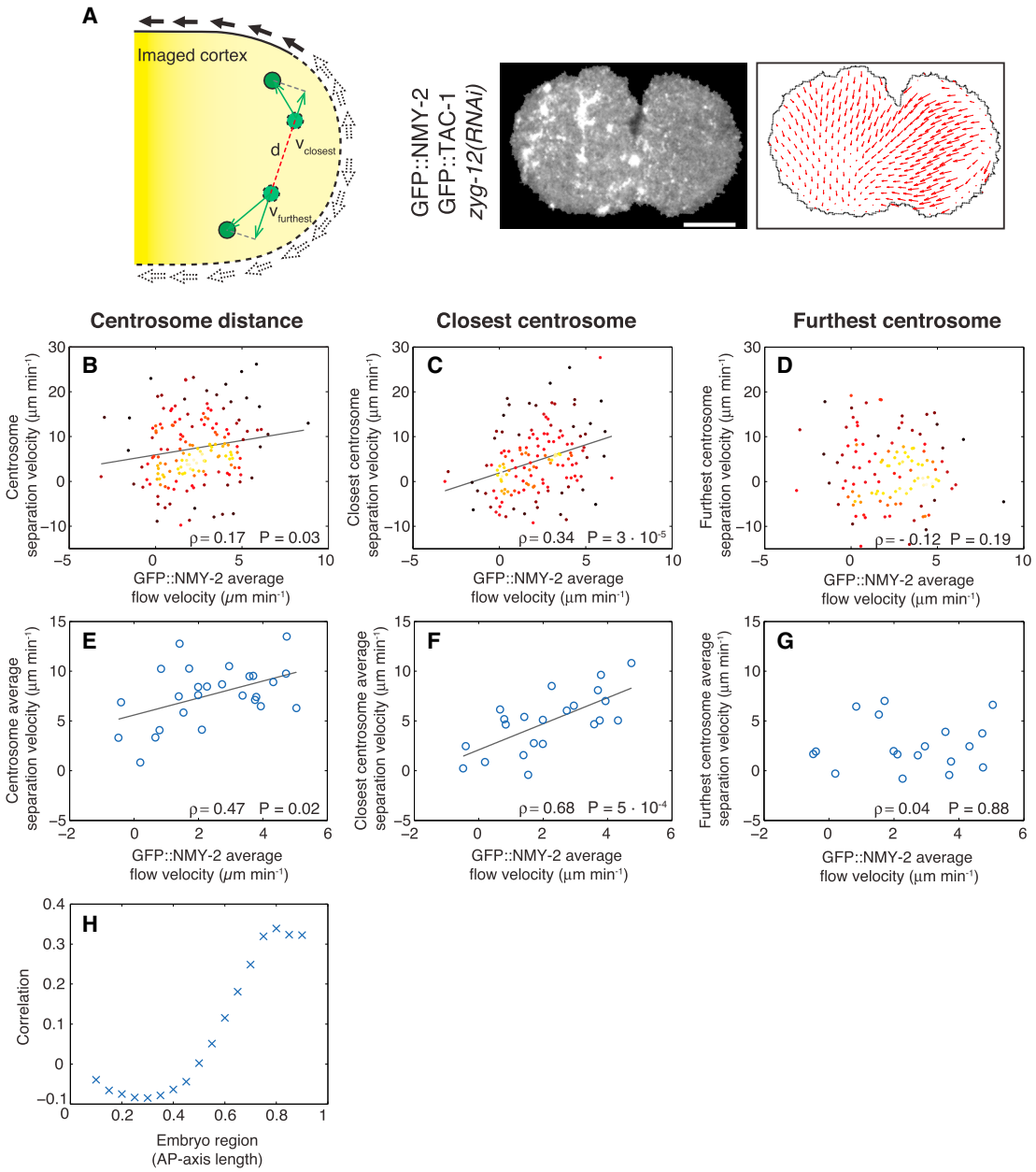

Figure 5. Actomyosin Cortex Flows Correlate with Separation Movements of the Closest Centrosome

(A) Schematic describing how the contribution of the movement of each centrosome to separation velocity was computed (left panel; see also Experimental Procedures). Imaging and PIV-derived measurement of GFP::NMY-2 cortical flows (two rightmost panels). In the PIV images, arrow direction and length represent flow direction and velocity, respectively (a.u.). Scale bar, 10 μm.

(B–D) A-P-directed velocities of the actomyosin cortical flow correlate with centrosome separation velocity measured at the same time (B) (n = 26; Pearson correlation coefficient, ρ = 0.17, p = 0.03, Student's t test); one outlier data point with cortical flow 11.2 μm min^{-1} and centrosome separation velocity 4.2 μm min^{-1} is not shown). Cortical flow velocity correlates with that of separation movements of the closest centrosome measured at the same time (C) (n = 22, ρ = 0.34, p = 3 • 10^{-5}; regression line with 95% confidence interval: slope = 1.3 [0.7–1.8], offset = 1.9 [0.3–3.5] μm min^{-1}; see Supplemental Experimental Procedures), but not with those of the furthest centrosome (D) (n = 18, ρ = −0.12, p = 0.19 [ns]). Data points are represented with a scale of color dependent on their spatial density in the scatterplot (a.u., from sparser to denser: dark red to yellow).

(E–G) Average posterior A-P-directed cortical flows correlate well with average centrosome separation velocity (E), n = 26; centrosome separation velocity, ρ = 0.47, p = 0.02), and correlate better with average separation movements of the closest centrosome (F) (n = 22; ρ = 0.68, p = 5 • 10^{-4}), but not with the average separation movements of the furthest centrosome (G) (n = 18; ρ = 0.04, p = 0.88 [ns]).

(H) Correlation between separation movements of the closest centrosome to the imaged cortical plane and cortical flows in different regions along embryo length. Each data point corresponds to the center of a region spanning 20% of total embryo length.

See also Movie S8.

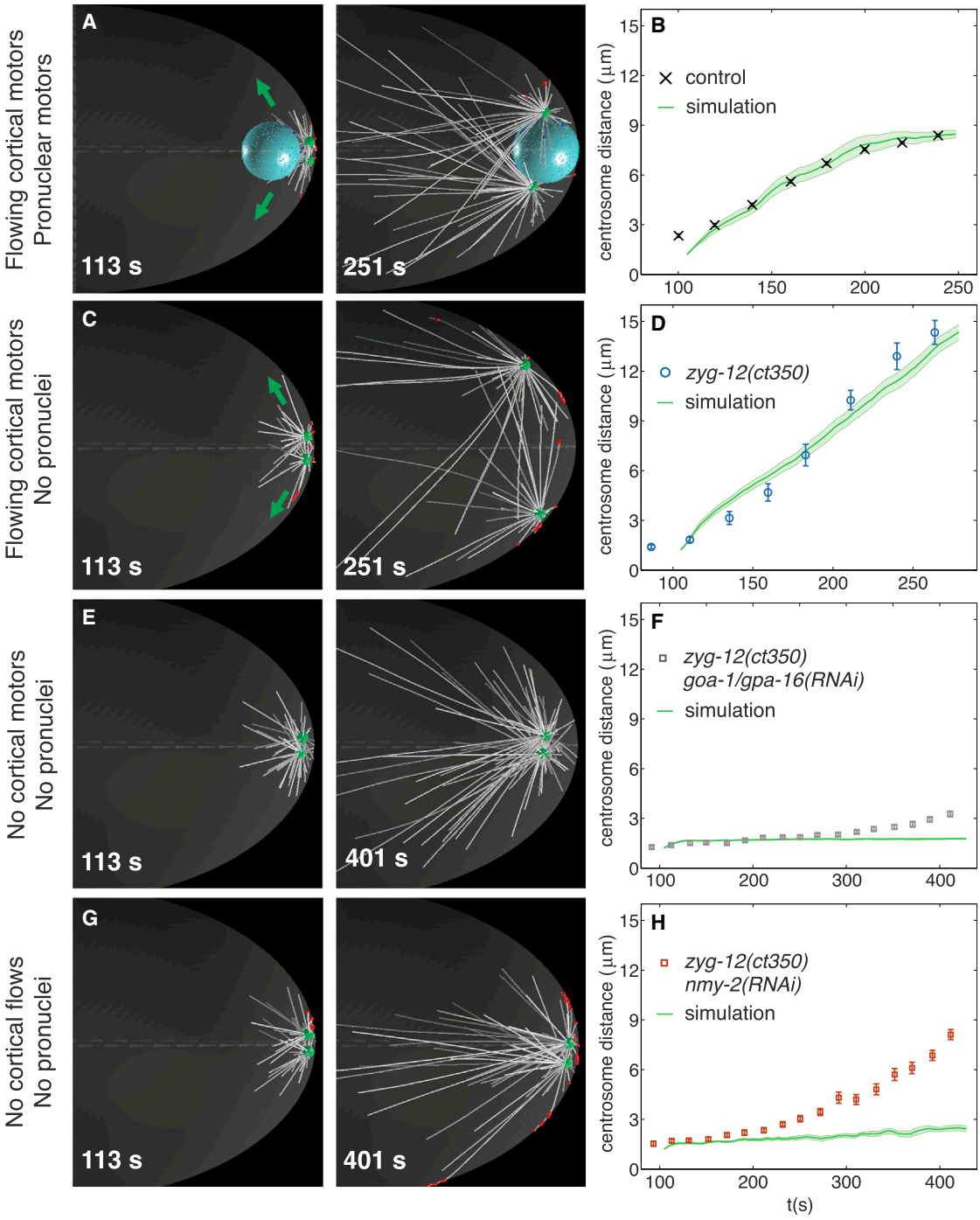

Figure 6. Computer Simulation of Centrosome Separation

(A, C, E, and G) Snapshots from computer simulation of centrosome separation are shown. Nuclear dynein (blue dots), cortical dynein (red dots), pronuclei (blue spheres), centrosomes (green dots), microtubules (white lines), and cortex (light gray ellipse in transparence) are depicted. For visual clarity, inactive motors are hidden, and only 1/4 microtubules are shown. Here and throughout the figure, the start of simulations corresponds to time, t, = 104 s of the synchronized experimental dataset.

(B, D, F, and H) The quantification of centrosome separation in computer simulations is compared with experimental data from indicated RNAi/mutant conditions with SEM (same as in Figures 2 and 3). Green curves: average simulated centrosome-centrosome distance with SEM (shaded error bars, n = 10) using the parameters given in Table S2. Note that while centrosomes show residual separation velocity in *zyg-12(ct350) nmy-2(RNAi)* (see Figure 3E), the computational model predicts that, in the absence of nuclear dynein and cortical flow, centrosome separation is completely impaired (Figure 6H). See the main text for a discussion of this point.

See also Figures S4–S6, Table S2, and Movies S9, S10, S11, S12, S13, S14, and S15.

along the cortex in the absence of nuclear motors (Figures 6C and 6D; Movie S10) and separate more slowly in the absence of cortical motors (Figures S4A and S4B; Movie S11).

We then addressed whether the parameter values thus selected could predict centrosome behavior in *zyg-12(ct350) goa-1/gpa-16(RNAi)*, *zyg-12(ct350) nmy-2(RNAi)*, and *nmy-2(RNAi)* embryos, which were not used for the fitting. Importantly, we found that simulations of all these conditions indeed predict with good quantitative agreement the observed centrosome separation behavior (Figures 6 and S4). Thus, no separation occurs when nuclear motors are depleted together with cortical motors (Figures 6E and 6F; Movie S12), whereas nuclear dynein can separate centrosomes, albeit at a slower pace, in the absence of cortical flows (Figures S4C and S4D; Movie S13). Moreover, in the computational model, the forces exerted by cortical dynein cannot drive centrosome separation on their own in the absence of cortical flows (Figures 6G and 6H; Movie S14). Importantly, in addition, we found that all the features of centrosome separation described in the computational model are robust to changes in motor densities at the nucleus and at the cortex (Figure S4E).

As an additional validation of the computational model, we tested whether it could predict the consequences of another condition that was not considered before. We chose to simulate embryos with smaller microtubule asters by reducing the rate of microtubule growth and increasing that of microtubule catastrophe; this led to slower centrosome separation than in control embryos (Figure S5A; Movie S15).To test our prediction experimentally, we imaged embryos depleted of the XMAP215 family protein ZYG-9, which have smaller microtubule asters (Matthews et al., 1998). Strikingly, we found that centrosomes separate more slowly in *zyg-9(RNAi)* embryos, in contrast to previous observations (Srayko et al., 2003) but in agreement with the predictions of our model (Figure S5B). Overall, we conclude that the computational model is a faithful and predictive representation of centrosome separation in one-cell stage *C. elegans* embryos.

Next, we set out to use the computational model to investigate whether binding of dynein to microtubules is sufficient to promote centrosome separation or whether dynein motor activity (i.e., motility) is needed in addition. First, as shown in Figures S6A and S6B, we found that rendering dynein non-motile prevents nuclear dynein-based centrosome separation, as anticipated. By contrast, we found that rendering dynein non-motile does not prevent cortical flow-based centrosome separation, although the process occurs at a slower pace than when dynein is motile (Figures S6C and S6D). Such a partial impairment might reflect the fact that, normally, cortical dynein motility favors the binding of additional motors to microtubules by pulling them toward the cortex.

Together, the computational simulations suggest that dynein functions in centrosome separation both as a motor protein from the nuclear envelope and as a cross-linker from the cortex to transmit forces deployed by flows, a role that is facilitated by motor activity.

DISCUSSION

Centrosome separation must be regulated in time and space to ensure faithful chromosome segregation (Silkworth et al., 2012). Our work indicates that centrosome separation in *C. elegans* embryos relies on the combined action of dynein at the nuclear envelope and dynein at the cell cortex, with the latter serving as a coupling device transmitting forces generated by the actomyosin network to microtubules emanating from centrosomes.

Previous work established that dynein is essential for, or contributes to, centrosome separation in a broad range of organisms, including *C. elegans*, *D. melanogaster*, and *H. sapiens* (reviewed in Tanenbaum and Medema, 2010). However, where in the cell, and through which mechanisms, dynein is required for this process in a physiological context was unclear from prior work. Here, by depleting dynein from the nucleus or from the cortex, we teased apart the distinct functions of these two pools of the motor protein to centrosome separation. By combining these experimental interrogations with computer simulations, we developed a model that explains how these two pools of dynein together separate centrosomes in a developing organism.

On the Role of Nuclear Dynein

Dynein at the nuclear envelope plays an important role in several processes in one-cell-stage *C. elegans* embryos. Thus, dynein tethered on the female pronucleus is thought to power its migration toward the male pronucleus by pulling along astral microtubules emanating from the centrosomes using its minus-end-directed motor activity (Gönczy et al., 1999). Our work reveals that, prior to that, dynein tethered on the male pronucleus plays a partially redundant role in centrosome separation, since this process can take place in the absence of cortical dynein, but at a slower pace. In other systems, slower centrosome separation leads to defects in chromosome attachment and error-prone chromosome segregation (Silkworth et al., 2012). Therefore, nuclear dynein might contribute to ensure genome integrity. Importantly, in addition, our analysis reveals that nuclear dynein not only maintains centrosomes in the vicinity of the nucleus (Malone et al., 2003; Robinson et al., 1999) but also prevents excess centrosome movements. Therefore, nuclear dynein is pivotal for proper temporal and spatial regulation of centrosome separation.

Cortical Dynein as a Coupling Device

Dynein anchored at the cell cortex exerts pulling forces on astral microtubules in several systems, including during spindle positioning in fungi, worms, and human cells (Vogel et al., 2009; reviewed in Kotak and Gönczy, 2013). Moreover, cortical dynein was proposed to mediate centrosome separation in *Drosophila* based on the presence of the motor protein at the cell cortex, although whether this is indeed the site from which the motor acts has not been tested in that system (Cytrynbaum et al., 2005; Sharp et al., 2000). By contrast, our work provides experimental evidence that cortical dynein is critical for centrosome separation.

Actomyosin contractility and cortical flows have been implicated in centrosome separation in vertebrate cells (Rosenblatt et al., 2004). This conclusion pertained to centrosome movements in a minority of cells in which separation occurs after nuclear envelope breakdown, and how flows were organized to drive outward centrosome movements was not clear. Moreover, how forces developed in the actomyosin network would be transmitted to

centrosomes was not known. Here, we show that when actomyosin contractility is compromised in *C. elegans*, cortical dynein-based centrosome separation is severely impaired. In principle, such impairment could be due to a reduction either in the cortical flows or in the rigidity of the actomyosin network, which could lead to the cortex not being able to sustain strong forces. Embryos depleted of NMY-2 and RHO-1 do not allow one to distinguish between these possibilities, as both flows and rigidity are compromised in these cases (Munro et al., 2004; Mayer et al., 2010; Redemann et al., 2011). By contrast, analysis of centrosome movements in *zyg-12(RNAi)* embryos expressing GFP::TAC-1 and GFP::NMY-2 shows that separation movements are proportional to the velocity of the neighboring cortical flows, even when actomyosin contractility is not altered. Alternatively, in principle, the impairment of centrosome separation upon depletion of NMY-2 or RHO-1 could reflect the reduction of cytoplasmic streaming that, in the wild-type, might exert forces on centrosomes through viscous drag. Cortical dynein could facilitate this process by pulling microtubules toward the cortex, where cytoplasmic flows are the fastest and thus exert maximal viscous drag force. However, we view this possibility as unlikely, because centrosomes do not move in the direction of cytoplasmic streaming when cortical and nuclear dynein are jointly depleted.

Computational simulations show also that cortical dynein, together with cortical flows, can separate centrosomes also when dynein motility is impaired. It will be interesting to test this prediction experimentally, for example, by impairing dynein motility through genome engineering of one of its AAA ATPase domains. Regardless, computational simulations indicate that the motor activity of cortical dynein contributes to centrosome separation in a less important manner, likely by pulling the microtubule aster toward the cortex, thus enhancing motor binding.

In conclusion, we propose a mechanism in which cortical dynein acts as a cross-linker that transmits forces generated by polarized flows of the actomyosin network to separate centrosomes. Remarkably, before their separation, centrosomes trigger a flow of the actomyosin network that is always directed away from them and that initiates the sequence of events leading to cell polarization (Bienkowska and Cowan, 2012; Goldstein and Hird, 1996; Munro et al., 2004). This cortical flow transports dynein motors anchored at the cortex, thus pulling the centrosomes apart, thereby coupling the initial events of cell polarization with centrosome separation. The cortical flow is initiated by the centrosomes themselves, thus guaranteeing mechanism robustness. We propose that this mechanism is broadly utilized to promote correct bipolar spindle assembly and thus ensure genome stability, including in tissue settings where cell volume is constrained by a compact geometry, with centrosomes being in close proximity to the actomyosin cortex.

EXPERIMENTAL PROCEDURES

Worm Strains

Transgenic worms expressing GFP::TAC-1 (Bellanger and Gönczy, 2003), GFP::AIR-1 (gift from Asako Sugimoto) (SA378; Toya et al., 2011), YFP::GPR-1 (strain TH242; gift from H. Bringmann) (Redemann et al., 2011), Lifeact::mKate2 (strain SWG001; gift from A.-C. Reymann and S. Grill) (Naganathan et al., 2014), and GFP::NMY-2 (strain JJ1473; gift from E. Munro) (Nance et al., 2003) were maintained at 24°C. Before analysis, the temperature-sensitive strain *zyg-12(ct350)* (Caenorhabditis Genetics Center) (Malone et al., 2003) was crossed with GFP::TAC-1, maintained at 16°C, and shifted to the restrictive temperature (24°C) for 1-4 hr or, when treated with RNAi, the duration indicated in the following text. Likewise, GFP::TAC-1 was crossed with GFP::NMY-2, and worms homozygous for both transgenes were maintained at 24°C. YFP::GPR-1 was crossed with Lifeact::mKate2, and worms homozygous for both transgenes were maintained at 24°C.

RNAi Bacterial Feeding

The RNAi feeding strains were obtained from the ORFeome RNAi library (a gift from M. Vidal) (Rual et al., 2004), except for *goa-1/gpa-16(RNAi)* (Colombo et al., 2003). RNAi was performed by feeding animals as follows: *goa-1/gpa-16(RNAi)* and *goa-1/gpa-16(RNAi) zyg-12 (ct350)*, by letting adults lay eggs on *goa-1/gpa-16(RNAi)* feeding plates and imaging the progeny of the F1 (first-filial-generation) animals after 134–163 hr at 16°C and then 1–4 hr at 24°C; *dhc-1(RNAi)*, for 15–17 hr at 24°C; *dhc-1(RNAi) zyg-12(ct350)*, for 42–47 hr at 16°C and then 1–4 hr at 24°C; *nmy-2(RNAi)* and *nmy-2(RNAi) zyg-12(ct350)*, for 42–47 hr at 16°C and then 1–4 hr at 24°C; *rho-1(RNAi) zyg-12(ct350)*, for 62–67 hr at 16°C and then 1–4 hr at 24°C; *zyg-12(RNAi)*, for 42–47 hr at 24°C. *zyg-9(RNAi)* was performed by feeding worms expressing GFP::AIR-1 for 48–56 hr at 24°C.

The efficiency of depletion by RNAi was assessed phenotypically as follows. For DHC-1, by the absence of centrosome movements, pronuclear migration, pronuclear and centrosome centration/rotation, and the depletion of minus-end-directed movements of yolk granules (Gönczy et al., 1999). For of GOA-1/GPA-16 and LIN-5, by the absence of spindle oscillations, and the impairment of spindle elongation/positioning was assessed during mitosis (Grill et al., 2001; Nguyen-Ngoc et al., 2007). For ZYG-12, by the detachment of centrosomes from the male pronucleus and the lack of pronuclear migration/meeting (Malone et al., 2003). For NMY-2 and RHO-1, by the impairment of cortical contractions and cortical flow (Motegi and Sugimoto, 2006; Shelton et al., 1999). The efficiency of ZYG-9 depletion via RNAi was assessed phenotypically by the impairment of pronuclear migration (Kemphues et al., 1986).

Centrosome and Pronuclear Tracking

Centrosomes were tracked in 3D using the Imaris Spot Detection feature (Bitplane) from the onset of separation until pronuclear meeting. In embryos where pronuclear meeting does not occur, the centrosomes were tracked until nuclear envelope breakdown. After synchronization with the control time reference (discussed later), centrosome separation curves were analyzed from the onset of separation to a time equivalent to that required for pronuclear meeting in the control ($t < 500$ s, referred to as "the equivalent time").

Pronuclei were tracked in 3D using a custom software written in MATLAB (MathWorks) based on the homogenous appearance of pronuclei with respect to the rough texture of the cytoplasm-containing yolk granules (Hamahashi et al., 2005) (Supplemental Experimental Procedures).

Centrosome Separation Curves Synchronization

To compare centrosome separation dynamics in different embryos, it is desirable to use a set time reference within the cell cycle. However, the time difference between centrosome separation onset and other cell-cycle progression landmarks detectable by DIC images (such as the end of meiosis II, pseudocleavage furrow ingression, pronuclear meeting, and nuclear envelope breakdown) was found to be variable, even in the control. Therefore, we synchronized centrosome separation curves in embryos within each experimental condition by maximizing the overall overlap of centrosome-centrosome distance curves (automatic overall minimization of mean squared deviation). Afterward, we used the aforementioned synchronization to calculate the mean male pronuclear size and found it to grow approximately linearly over time. Thus, we used the average male pronucleus size as a reference to compare the mean separation curves from different experimental conditions. For every condition, we calculated a time shift by minimizing the mean squared deviation of the male pronucleus size curves between the given condition and the control; thereafter, we applied this time shift to the centrosome trajectories of the given condition. In such a synchronization, the control is used as a reference and time 0 s is defined as the earliest time point at which two distinct

centrosomes could be detected in the whole synchronized control dataset. All the centrosome separation curves presented here have been synchronized using this procedure, thus allowing comparison of the timescale between different figures.

Cortical Flow Measurements and Cortical Flow-Centrosome Separation Correlation Analysis

Cortical flows were measured using PIV as previously described (Mayer et al., 2010). PIV was performed using the MATLAB-based MPIV toolbox (Nobuhito and Kuang-An, 2003) and the Minimum Quadric Difference algorithm (see Supplemental Experimental Procedures for details).

For the correlation analysis between cortical flows and centrosome separation velocities, the reference flow velocity at each time point was computed by averaging flow velocity vectors within 70%–90% of embryo length (0%, anterior-most; 100%, posterior-most). Centrosomes were tracked in 3D using the Imaris Spot Detection feature (Bitplane). To select the phase during which centrosomes separate at approximately constant velocity, we considered only frames in which the centrosomes were separated by a distance between 3 and 12 μm. For the correlation analysis of the separation movements of the closest and furthest centrosomes, considering that, in our experimental conditions, the whole embryo height is approximately 20 μm, we conducted this analysis only on those embryos in which the closest centrosome was <8 μm from the imaged cortical plane at the end of the movie. Conversely, the furthest centrosome was retained for correlation analysis only if it was located >12 μm from the imaged cortical section at the end of the movie.

The velocity of the separation movements of the centrosomes was computed as in (Waters et al., 1993)

$$v_{\text{closest}} = \frac{(\mathbf{x}_{\text{closest}}(t+1) - \mathbf{x}_{\text{closest}}(t)) \bullet (\mathbf{x}_{\text{closest}}(t) - \mathbf{x}_{\text{furthest}}(t))}{\|\mathbf{x}_{\text{closest}}(t) - \mathbf{x}_{\text{furthest}}(t)\|}$$
$$v_{\text{furthest}} = \frac{(\mathbf{x}_{\text{furthest}}(t+1) - \mathbf{x}_{\text{furthest}}(t)) \bullet (\mathbf{x}_{\text{furthest}}(t) - \mathbf{x}_{\text{closest}}(t))}{\|\mathbf{x}_{\text{furthest}}(t) - \mathbf{x}_{\text{closest}}(t)\|}, \quad (1)$$

where $\mathbf{x}(t)$ is the position of the indicated centrosome at frame t (Figure 5A).

Computer Simulation

Computer simulations were performed using Cytosim (Nedelec and Foethke, 2007). In brief, overdamped Langevin equations are used to describe the motion of elastic fibers and solids in a viscous fluid in the presence of Brownian motion. All stochastic events (motor binding, catastrophes, and nucleation) are generated as first-order random events. The simulation parameters are summarized in Table S2. The embryo is simulated as an ellipsoid, 50 × 30 × 30 μm, with the cytoplasm having homogenous constant viscosity. The cell cortex is considered to be the embryo boundary that confines microtubules, centrosomes, and pronuclei. A soft excluded volume interaction applies to centrosomes, microtubules, and pronuclei, preventing these objects from overlapping, except that microtubule-microtubule interactions are not considered.

Microtubules and Centrosomes

Centrosomes and microtubules are simulated as described previously (Kozlowski et al., 2007). In brief, microtubules are flexible fibers that follow a two-state dynamic instability model. Shrinkage rate is constant, and growth rate is reduced by antagonistic force: $v = v_g \exp(f/f_g)$ if the projected force, f, is negative, and $v = v_g$ otherwise (Table S2). The catastrophe rate depends on whether the microtubule tip touches the cortex or is in the cytoplasm, and it is also induced by force as described previously (Foethke et al., 2009). When a microtubule depolymerizes completely, it is removed from the simulation. Centrosomes are spheres of 1 μm in diameter, covered by microtubule nucleation sites. Empty nucleation sites can lead to the nucleation of a microtubule with a constant probability and, subsequently, remain inactive until this microtubule depolymerizes entirely.

Pronuclei

The pronuclei are simulated as spherical objects as described previously (Foethke et al., 2009). Pronuclei can move, rotate, and grow in size at a constant rate. During centrosome separation in vivo, the female pronucleus drifts slowly toward the posterior, before it accelerates to meet the male pronucleus. The early drift is likely not due to interactions with the microtubule asters, since it still occurs when centrosomal microtubule nucleation is impaired (for example, in *spd-5(RNAi)*) (Hamill et al., 2002). We modeled this drift by adding an effective force directed toward the posterior acting on the female pronucleus.

Dynein Motors

Individual minus-directed dynein complexes are simulated as described previously (Rupp and Nédélec, 2012). In brief, dynein motors have a base fixed on the pronucleus or at the cortex and can bind to microtubules that are within their binding range. A bound dynein motor exerts a force between the base and the attachment point on the microtubule that is Hookean with zero resting length. Motor unbinding depends on the applied force f as $k_{\text{off}} = k_u e^{f/f_u}$, and the force-velocity relationship is $v = v_0(1 - f/f_s)$ (Table S2).

The density of motors on the surface of the pronuclei is constant, and inactive motors can bind microtubules within their binding range with a certain rate. Cortical motors are considered to be in excess and homogenously distributed on the cell cortex, so that only active cortical motors are simulated. When a microtubule tip touches the cortex, with a certain capture rate, an active cortical dynein motor is created in the simulation and attached to the microtubule. Each microtubule can bind multiple dynein motors simultaneously. When a cortical dynein motor detaches from the microtubule, it is removed from the simulation.

The effect of cortical flow is implemented by displacing the anchor points of the cortical motors away from the posterior side with a speed tangent to the cortex. The flow linearly increases from the anterior to the posterior side along the A-P embryonic axis to reflect the situation in the embryo (Mayer et al., 2010; Munro et al., 2004). The flow does not have any twist component with respect to the A-P axis.

Initial Condition

At the start of the simulation, the male and female pronuclei are at the presumptive posterior and anterior sides of the embryos, respectively. The centrosomes are located between the male pronucleus and the posterior cortex. The initial centrosome-centrosome distance is 1.2 μm. No microtubules are polymerized, and all dynein motors are unbound.

Parameter Fit

Two parameter values were derived from a fit to the experimental data: pronuclear motor density and cortical motor capture rate. The objective of the fit was to simultaneously match centrosome distance curves in control, *zyg-12(ct350)*, and *goa-1/gpa-16(RNAi)* conditions. To this end, we minimized the total χ^2, defined as the sum of integrals of the squared differences (weighted by the inverse of the squared SEM of the experimental average curves) between the average of ten independent simulations and the experimental average curves.

SUPPLEMENTAL INFORMATION

Supplemental Information includes Supplemental Experimental Procedures, six figures, two tables, and 15 movies and can be found with this article online at http://dx.doi.org/10.1016/j.celrep.2016.01.077.

AUTHOR CONTRIBUTIONS

A.D. and P.G. designed the project; A.D. conducted experiments; A.D. and P.G. analyzed data; A.D. and P.G. designed the computational model; A.D. and F.N. developed the simulation; A.D. and P.G. wrote the manuscript.

ACKNOWLEDGMENTS

We thank Aitana Neves da Silva for help in developing the script for tracking pronuclei, Simon Blanchoud for scripts and advice as well as Christian Gentili, Stephan Grill, Félix Naef, and Sachin Kotak for advice; and Alexander Mogilner, Virginie Hamel, Aitana Neves da Silva, and Sachin Kotak for comments on the manuscript. For strains, we thank Asako Sugimoto, Henrik Bringmann, Ed Munro, Anne-Cécile Reymann, and Stephan Grill, as well as the Caenorhabditis Genetics Center, which is funded by the NIH National Center for Research Resources (NCRR).

This work was supported by the Swiss National Science Foundation (3100A0-122500/1 and 31003A_155942). The funders had no role in study design, data collection and analysis, decision to publish, or preparation of the manuscript.

Received: November 5, 2015
Revised: December 23, 2015
Accepted: January 27, 2016
Published: February 25, 2016

REFERENCES

Bellanger, J.M., and Gönczy, P. (2003). TAC-1 and ZYG-9 form a complex that promotes microtubule assembly in C. elegans embryos. Curr. Biol. *13*, 1488–1498.

Bienkowska, D., and Cowan, C.R. (2012). Centrosomes can initiate a polarity axis from any position within one-cell *C. elegans* embryos. Curr. Biol. *22*, 583–589.

Cao, J., Crest, J., Fasulo, B., and Sullivan, W. (2010). Cortical actin dynamics facilitate early-stage centrosome separation. Curr. Biol. *20*, 770–776.

Colombo, K., Grill, S.W., Kimple, R.J., Willard, F.S., Siderovski, D.P., and Gönczy, P. (2003). Translation of polarity cues into asymmetric spindle positioning in *Caenorhabditis elegans* embryos. Science *300*, 1957–1961.

Cytrynbaum, E.N., Sommi, P., Brust-Mascher, I., Scholey, J.M., and Mogilner, A. (2005). Early spindle assembly in Drosophila embryos: role of a force balance involving cytoskeletal dynamics and nuclear mechanics. Mol. Biol. Cell *16*, 4967–4981.

Dujardin, D.L., and Vallee, R.B. (2002). Dynein at the cortex. Curr. Opin. Cell Biol. *14*, 44–49.

Ferenz, N.P., Gable, A., and Wadsworth, P. (2010). Mitotic functions of kinesin-5. Semin. Cell Dev. Biol. *21*, 255–259.

Foethke, D., Makushok, T., Brunner, D., and Nédélec, F. (2009). Force- and length-dependent catastrophe activities explain interphase microtubule organization in fission yeast. Mol. Syst. Biol. *5*, 241.

Goldstein, B., and Hird, S.N. (1996). Specification of the anteroposterior axis in *Caenorhabditis elegans*. Development *122*, 1467–1474.

Gönczy, P., Pichler, S., Kirkham, M., and Hyman, A.A. (1999). Cytoplasmic dynein is required for distinct aspects of MTOC positioning, including centrosome separation, in the one cell stage *Caenorhabditis elegans* embryo. J. Cell Biol. *147*, 135–150.

Gotta, M., and Ahringer, J. (2001). Distinct roles for Galpha and Gbetagamma in regulating spindle position and orientation in *Caenorhabditis elegans* embryos. Nat. Cell Biol. *3*, 297–300.

Gotta, M., Dong, Y., Peterson, Y.K., Lanier, S.M., and Ahringer, J. (2003). Asymmetrically distributed *C. elegans* homologs of AGS3/PINS control spindle position in the early embryo. Curr. Biol. *13*, 1029–1037.

Grill, S.W., Gönczy, P., Stelzer, E.H., and Hyman, A.A. (2001). Polarity controls forces governing asymmetric spindle positioning in the *Caenorhabditis elegans* embryo. Nature *409*, 630–633.

Hamahashi, S., Onami, S., and Kitano, H. (2005). Detection of nuclei in 4D Nomarski DIC microscope images of early Caenorhabditis elegans embryos using local image entropy and object tracking. BMC Bioinformatics *6*, 125.

Hamill, D.R., Severson, A.F., Carter, J.C., and Bowerman, B. (2002). Centrosome maturation and mitotic spindle assembly in *C. elegans* require SPD-5, a protein with multiple coiled-coil domains. Dev. Cell *3*, 673–684.

Kemphues, K.J., Wolf, N., Wood, W.B., and Hirsh, D. (1986). Two loci required for cytoplasmic organization in early embryos of *Caenorhabditis elegans*. Dev. Biol. *113*, 449–460.

Kimura, A., and Onami, S. (2005). Computer simulations and image processing reveal length-dependent pulling force as the primary mechanism for *C. elegans* male pronuclear migration. Dev. Cell *8*, 765–775.

Kotak, S., and Gönczy, P. (2013). Mechanisms of spindle positioning: cortical force generators in the limelight. Curr. Opin. Cell Biol. *25*, 741–748.

Kozlowski, C., Srayko, M., and Nedelec, F. (2007). Cortical microtubule contacts position the spindle in C. elegans embryos. Cell *129*, 499–510.

Le Bot, N., Tsai, M.C., Andrews, R.K., and Ahringer, J. (2003). TAC-1, a regulator of microtubule length in the *C. elegans* embryo. Curr. Biol. *13*, 1499–1505.

Lorson, M.A., Horvitz, H.R., and van den Heuvel, S. (2000). LIN-5 is a novel component of the spindle apparatus required for chromosome segregation and cleavage plane specification in Caenorhabditis elegans. J. Cell Biol. *148*, 73–86.

Malone, C.J., Misner, L., Le Bot, N., Tsai, M.C., Campbell, J.M., Ahringer, J., and White, J.G. (2003). The *C. elegans* hook protein, ZYG-12, mediates the essential attachment between the centrosome and nucleus. Cell *115*, 825–836.

Matthews, L.R., Carter, P., Thierry-Mieg, D., and Kemphues, K. (1998). ZYG-9, a *Caenorhabditis elegans* protein required for microtubule organization and function, is a component of meiotic and mitotic spindle poles. J. Cell Biol. *141*, 1159–1168.

Mayer, M., Depken, M., Bois, J.S., Jülicher, F., and Grill, S.W. (2010). Anisotropies in cortical tension reveal the physical basis of polarizing cortical flows. Nature *467*, 617–621.

Motegi, F., and Sugimoto, A. (2006). Sequential functioning of the ECT-2 RhoGEF, RHO-1 and CDC-42 establishes cell polarity in *Caenorhabditis elegans* embryos. Nat. Cell Biol. *8*, 978–985.

Munro, E., Nance, J., and Priess, J.R. (2004). Cortical flows powered by asymmetrical contraction transport PAR proteins to establish and maintain anterior-posterior polarity in the early *C. elegans* embryo. Dev. Cell *7*, 413–424.

Naganathan, S.R., Fürthauer, S., Nishikawa, M., Jülicher, F., and Grill, S.W. (2014). Active torque generation by the actomyosin cell cortex drives left-right symmetry breaking. eLife *3*, e04165.

Nance, J., Munro, E.M., and Priess, J.R. (2003). *C. elegans* PAR-3 and PAR-6 are required for apicobasal asymmetries associated with cell adhesion and gastrulation. Development *130*, 5339–5350.

Nedelec, F., and Foethke, D. (2007). Collective Langevin dynamics of flexible cytoskeletal fibers. New J. Phys. *9*, 427.

Nguyen-Ngoc, T., Afshar, K., and Gönczy, P. (2007). Coupling of cortical dynein and G alpha proteins mediates spindle positioning in *Caenorhabditis elegans*. Nat. Cell Biol. *9*, 1294–1302.

Nobuhito, M., and Kuang-An, C. (2003). Introduction to MPIV, user reference manual. http://www.oceanwave.jp/softwares/mpiv.

Raaijmakers, J.A., van Heesbeen, R.G., Meaders, J.L., Geers, E.F., Fernandez-Garcia, B., Medema, R.H., and Tanenbaum, M.E. (2012). Nuclear envelope-associated dynein drives prophase centrosome separation and enables Eg5-independent bipolar spindle formation. EMBO J. *31*, 4179–4190.

Redemann, S., Schloissnig, S., Ernst, S., Pozniakowsky, A., Ayloo, S., Hyman, A.A., and Bringmann, H. (2011). Codon adaptation-based control of protein expression in *C. elegans*. Nat. Methods *8*, 250–252.

Reinsch, S., and Gönczy, P. (1998). Mechanisms of nuclear positioning. J. Cell Sci. *111*, 2283–2295.

Robinson, J.T., Wojcik, E.J., Sanders, M.A., McGrail, M., and Hays, T.S. (1999). Cytoplasmic dynein is required for the nuclear attachment and migration of centrosomes during mitosis in *Drosophila*. J. Cell Biol. *146*, 597–608.

Rose, L., and Gönczy, P. (2014). Polarity establishment, asymmetric division and segregation of fate determinants in early *C. elegans* embryos. WormBook, 1–43.

Rosenblatt, J., Cramer, L.P., Baum, B., and McGee, K.M. (2004). Myosin II-dependent cortical movement is required for centrosome separation and positioning during mitotic spindle assembly. Cell *117*, 361–372.

Rual, J.F., Ceron, J., Koreth, J., Hao, T., Nicot, A.S., Hirozane-Kishikawa, T., Vandenhaute, J., Orkin, S.H., Hill, D.E., van den Heuvel, S., and Vidal, M. (2004). Toward improving Caenorhabditis elegans phenome mapping with an ORFeome-based RNAi library. Genome Res. *14* (*10B*), 2162–2168.

Rupp, B., and Nédélec, F. (2012). Patterns of molecular motors that guide and sort filaments. Lab Chip *12*, 4903–4910.

Saunders, A.M., Powers, J., Strome, S., and Saxton, W.M. (2007). Kinesin-5 acts as a brake in anaphase spindle elongation. Curr. Biol. *17*, R453–R454.

Sharp, D.J., Brown, H.M., Kwon, M., Rogers, G.C., Holland, G., and Scholey, J.M. (2000). Functional coordination of three mitotic motors in *Drosophila* embryos. Mol. Biol. Cell *11*, 241–253.

Shelton, C.A., Carter, J.C., Ellis, G.C., and Bowerman, B. (1999). The non-muscle myosin regulatory light chain gene mlc-4 is required for cytokinesis, anterior-posterior polarity, and body morphology during *Caenorhabditis elegans* embryogenesis. J. Cell Biol. *146*, 439–451.

Silkworth, W.T., Nardi, I.K., Paul, R., Mogilner, A., and Cimini, D. (2012). Timing of centrosome separation is important for accurate chromosome segregation. Mol. Biol. Cell *23*, 401–411.

Splinter, D., Tanenbaum, M.E., Lindqvist, A., Jaarsma, D., Flotho, A., Yu, K.L., Grigoriev, I., Engelsma, D., Haasdijk, E.D., Keijzer, N., et al. (2010). Bicaudal D2, dynein, and kinesin-1 associate with nuclear pore complexes and regulate centrosome and nuclear positioning during mitotic entry. PLoS Biol. *8*, e1000350.

Srayko, M., Quintin, S., Schwager, A., and Hyman, A.A. (2003). *Caenorhabditis elegans* TAC-1 and ZYG-9 form a complex that is essential for long astral and spindle microtubules. Curr. Biol. *13*, 1506–1511.

Srinivasan, D.G., Fisk, R.M., Xu, H., and van den Heuvel, S. (2003). A complex of LIN-5 and GPR proteins regulates G protein signaling and spindle function in *C elegans*. Genes Dev. *17*, 1225–1239.

Tanenbaum, M.E., and Medema, R.H. (2010). Mechanisms of centrosome separation and bipolar spindle assembly. Dev. Cell *19*, 797–806.

Tikhonenko, I., Nag, D.K., Martin, N., and Koonce, M.P. (2008). Kinesin-5 is not essential for mitotic spindle elongation in Dictyostelium. Cell Motil. Cytoskeleton *65*, 853–862.

Toya, M., Terasawa, M., Nagata, K., Iida, Y., and Sugimoto, A. (2011). A kinase-independent role for Aurora A in the assembly of mitotic spindle microtubules in *Caenorhabditis elegans* embryos. Nat. Cell Biol. *13*, 708–714.

Tsou, M.-F.B., Hayashi, A., DeBella, L.R., McGrath, G., and Rose, L.S. (2002). LET-99 determines spindle position and is asymmetrically enriched in response to PAR polarity cues in *C. elegans* embryos. Development *129*, 4469–4481.

Vogel, S.K., Pavin, N., Maghelli, N., Jülicher, F., and Tolić-Nørrelykke, I.M. (2009). Self-organization of dynein motors generates meiotic nuclear oscillations. PLoS Biol. *7*, 0918–0928.

Waters, J.C., Cole, R.W., and Rieder, C.L. (1993). The force-producing mechanism for centrosome separation during spindle formation in vertebrates is intrinsic to each aster. J. Cell Biol. *122*, 361–372.